NUMERICAL SOLUTION OF 3–D TURBULENT FLOWS INSIDE OF NEW CONCEPT NOZZLES

Zheng Xiaoqing
Chinese Academy of Sciences,Institute of Engineering Thermophysics
P.O.Box 2706,Beijing 100080,P.R.China
Zhang Mingheng, Lai Chuanxin, Jin Hui and Zen Jun
Gas Turbine Establishment of Aviation and Space Ministry of China
P.O. Box 305,Jiang You, Sichuan 621703, P.R.China

Abstract

This paper presents a numerical method for calculating the internal flow field of circular–to–rectangular transition ducts and nonaxisymmetric nozzles. This analysis, based on the solution of N–S equations with time marching scheme, is capable of predicting the internal three dimensional turbulent flows. To improve the computational efficiency and alleviate the requirement for huge computer storage, a new finite volume approach for viscous terms in 3–D case is proposed. The B–L turbulence model is used to estimate the Reynolds stresses. The definition of the mixing length of turbulent flow in the vicinity of wall corner is suggested. The principle for choosing the eddy–viscosity is also established. An original method for generating high–performance grid inside duct is developed through analytic transformation. It is ideal to all shapes from circular to rectangular section for its excellent natures of orthogonality and controllability.

Three transition ducts with different lengths connected with a convergent–divergent nozzle is investigated in present paper. Numerical results surprisingly accurately match the test data in all cases, demonstrating the accuracy and capability of present method.

Introduction

For designer of future jet–engine exhaust system, more and more interests are focused on the multifunction nonaxisymmetric nozzles. Its remarkable character in reducing infrared radiation and significant capability of vectoring / reversing are very important for innovative manoeuvrable, stealthy aeroplane. However the rectangular shape of nozzle has create the design problem of transitioning the axisymmetric engine flow to the nonaxisymmetric nozzle flow, though the geometric smoothness of transition duct from circular to rectangular could be achieved by connecting a series of superellipse cross section. The duct length is a key dimension to be determined for a given aspect–ratio. With a view to minimizing the weight of the propulsion system installation, the duct should be as short as possible. On the otherside it must also be long enough to prevent any separation for which could cause severe cooling problem and significant internal performance loss. Therefore, both experimental and numerical investigations are intensely conducted in recent years to determine the overall performance of circular–to–rectangular so as to explore the effect of duct dimensions on the performance [1,2,3,4]. Though tunnel tests could provide reliable results, numerical modelling is appealing for its lower cost and higher efficiency. Unfortunately, because of the highly viscous nature of the flow inside the transition duct, potential–flow solution and Euler solution are incapable of accurately matching the experimental data. So the viscous effects must be included in the numerical code. This paper presents a numerical method capable of predicting the internal 3–D turbulent flows and access the effects of duct length on nozzle performance. A new finite volume scheme for the discretization of viscous terms is proposed to have the advantage over previous method of less demand for storage and speed of computers. Special care is payed to the implement of turbulence model in 3–D flow computation.

For transition ducts, to maintain a high performance, the cross section shape is required to change from circular to rectangular through a smooth and rapid progression. This creates the difficulty of grid generation, because the grid structure fitting well to rectangle may be unacceptable for the circle. To overcome this difficulty, an original method for generating high quality grid analytically inside ducts is contrived. It is suitable for all shapes of superellipse and easy to be extended to the general duct.

Numerical investigation is conducted on the 3–D turbulent flow fields of three transition ducts integrated with a nonaxisymmetric nozzle. Both Euler solver and N–S solver are used. As expected, the N–S solver gives excellent results for all cases while the Euler solutions have a big deviation from the experimental data in region where the viscosity becomes dominating, say sepa-

ration occurred. To have a insight into the flow patterns in the transition duct, the 3d view pictures of the near-surface velocity vector , calculated using N-S equations, are plotted. The separation pattern in some of the configurations is fully demonstrated. The computational results are satisfactory in congruity with the test and helpful to the understanding the flow phenomena inside of the ducts.

Governing Equations

The three dimensional Navier-Stokes equations in integration form are

$$\left.\begin{aligned}
&\int_\Omega \frac{\partial \rho}{\partial t} d\Omega + \int_\Gamma \rho(\vec{q}\cdot\vec{ds}) = 0\\
&\int_\Omega \frac{\partial \rho\vec{q}}{\partial t} d\Omega + \int_\Gamma \rho\vec{q}(\vec{q}\cdot\vec{ds}) = \int_\Gamma \vec{\tau}_s ds\\
&\int_\Omega \frac{\partial e}{\partial t} d\Omega + \int_\Gamma e(\vec{q}\cdot\vec{ds}) = \int_\Gamma (\vec{\tau}_s\cdot\vec{q}) ds\\
&\qquad\qquad + \int_\Gamma c\left(\frac{\partial (p/\rho)}{\partial n}\right) ds\\
&p = (K-1)(e - \frac{1}{2}\rho q^2)\\
&[\tau] = -\left(P + \frac{2}{3}\mu \mathrm{div}\cdot(\vec{q})\right)[I] + 2\mu[\varepsilon]
\end{aligned}\right\} \quad (1)$$

$$C = \frac{K}{K-1}\left(\frac{\mu_e}{p_{re}} + \frac{\mu_t}{p_{rt}}\right)$$

where Ω denotes a fixed region with boundary Γ, $\vec{q}$ represents velocity, ρ is density, p is pressure, e stands for total energy per unit volume, τ_s is the viscous stress acted on the plane ds with outer normal $\vec{n}$, K is ratio of specific heats, p_r is Prandtl number.

The effective viscosity coefficient μ in turbulent flow computation is the sum of the molecular viscosity μ_c and the eddy viscosity μ_t. The variation with temperature of the molecular viscosity μ_c is determined using Sutherland's law, while the eddy viscosity coefficient μ_t is determined by use of the algebraic model proposed by Baldwin-Lomax[5]. The modification of this two-layer mode to three dimensional case is studied in present study and discribed in the later section.

Solution Method

The computational domain is divided into hexahedral cells, and the variables are defined at cell centre (i,j,k). The integrals in equ.(1) are replaced by discrete summation around the faces (numbered as l) of the cell:

$$\left.\begin{aligned}
\frac{d\rho}{dt} &= -\frac{1}{Vol}\sum \rho_l(\vec{q}\cdot\vec{S})_l\\
\frac{d(\rho u)}{dt} &= -\frac{1}{Vol}[\sum(\rho u)_l(\vec{q}\cdot\vec{S})_l + \sum \hat{p}_l S_{lx} + \sum(Fx\ S)_l]\\
\frac{d(\rho v)}{dt} &= -\frac{1}{Vol}[\sum(\rho v)_l(\vec{q}\cdot\vec{S})_l + \sum \hat{p}_l S_{ly} + \sum(Fy\ S)_l]\\
\frac{d(\rho w)}{dt} &= -\frac{1}{Vol}[\sum(\rho w)_l(\vec{q}\cdot\vec{S})_l + \sum \hat{p}_l S_{lz} + \sum(Fz\ S)_l]\\
\frac{d(\rho e)}{dt} &= -\frac{1}{Vol}[\sum(\rho e)_l(\vec{q}\cdot\vec{S})_l + \sum \hat{p}_l(\vec{q}\cdot\vec{S}) + \sum(\vec{F}\cdot\vec{q})S]
\end{aligned}\right\} \quad (4)$$

where Vol is cell volume, $\vec{S}_l = (S_{lx}, S_{ly}, S_{lz})^T$ is the area vector of cell face. u,v and w are velocity components in x,y,z direction respectively. $\vec{F} = (Fx, Fy, Fz)^T$ and $\hat{p}$ are viscous stress, which will be discussed in later section.

The semi-discretization equations (4) are solved using the modified multi-stage Runge-Kutta time marching scheme[6]. The acceleration techniques such as implicit residual averaging are used.

New Approach to Viscous Terms

In previous methods, the shear stress is needed to calculate at each of the six faces of one cell (at least three faces) . It is computational costly very much. There have been much efforts made towards achieving solution efficiency by simplification, however most of those methods suffered non-conservation problem. A new scheme is proposed in [4] by the first author to eliminates above mentioned problems. This method has applied to the two dimensional turbulent flow computation [7,8] and proven very successful. Here we derive the three dimensional version in detail.

In local cartesian Coordinates (n,ζ,η) , the shear stress at the face between (i,j,k) and (i+1,j,k) has the form:

$$\left\{\begin{aligned}
\tau_n &= -p + 2\mu\frac{\partial q_n}{\partial n} - \frac{2}{3}\mu\,\mathrm{div}\,\vec{q}\\
\tau_\zeta &= \mu\left(\frac{\partial q_n}{\partial \zeta} + \frac{\partial q_\zeta}{\partial n}\right)\\
\tau_\eta &= \mu\left(\frac{\partial q_n}{\partial \eta} + \frac{\partial q_\eta}{\partial n}\right)
\end{aligned}\right. \quad (5)$$

Where q_n, q_ζ, q_η is the velocity componentin n, ζ, η direction respectively.

By Setting $\hat{p} = p + \frac{2}{3}\mu\mathrm{div}\cdot(\vec{q})$, the shear stress can be divided into:
normal stress:

$$\vec{F}_n = \tau_n\vec{n} = \left(-\hat{p} + 2\mu\frac{\partial q_n}{\partial n}\right)\vec{n} \quad (6a)$$

and tangential stress:

$$F_T = \tau_\zeta\vec{\zeta} + \tau_\eta\vec{\eta} = \mu\left(\frac{\partial \vec{q}_T}{\partial n}\right) + \mu\,\mathrm{grad}_T\, q_n \quad (6b)$$

Where $\vec{u}_T = q_\zeta\vec{\zeta} + q_\eta\vec{\eta}$, and

$$\mathrm{grad}_T = \vec{\zeta}\frac{\partial}{\partial\zeta} + \vec{\eta}\frac{\partial}{\partial\eta}$$

is the gradient operated on (ζ,η) plane.

If we take $\hat{p}$ out and regard it as pressure, the remainder is:

$$\vec{F} = \vec{F}_T + 2\frac{\partial q_n}{\partial n}\vec{n} = \mu\frac{\partial\vec{q}}{\partial n} + \mu\,\mathrm{grad}\,q_n \quad (7)$$

Here $\mathrm{grad} = \vec{n}\frac{\partial}{\partial n} + \vec{\zeta}\frac{\partial}{\partial\zeta} + \vec{\eta}\frac{\partial}{\partial\eta}$.

Equ.(7) is actually a general vector form of deviatoric stress, however it is still not suitable for calculation . We now cast it into finite volume scheme in global Cartesian coordinate system (x,y,z).

Since: $q_n = \vec{q} \cdot \vec{n} = un_x + vn_y + wn_z$

$$\frac{\partial \vec{q}}{\partial n} = \vec{i}\frac{\partial u}{\partial n} + \vec{j}\frac{\partial v}{\partial n} + \vec{k}\frac{\partial w}{\partial n}$$

therefore

$$\text{grad } q_n = n_x \text{ grad } u + n_y \text{ grad } v + n_z \text{ grad } w \tag{8}$$

$$\frac{\partial \vec{q}}{\partial n} = \vec{i}(\vec{n} \cdot \text{grad } u) + \vec{j}(\vec{n} \cdot \text{grad } v) + \vec{k}(\vec{n} \cdot \text{grad } w) \tag{9}$$

Utilizing (8) and (9), rewrite (7) as:

$$\begin{aligned}\vec{F} = \mu[&n_x \text{grad } u + n_y \text{ grad } v + n_z \text{ grad } w \\ &+ \vec{i}(\vec{n} \cdot \text{grad } u) + \vec{j}(\vec{n} \cdot \text{grad } v) \\ &+ \vec{k}(\vec{n} \cdot \text{grad } w)]\end{aligned} \tag{10}$$

Now we need to compute gradients of three velocity components to determine shear stress. It is still too expensive for computation in present form, further deduction is needed.

According to finite volume formula:

$$u = \frac{1}{2}(u_{i,j,k} + u_{i+1,j,k})$$

$$v = \frac{1}{2}(v_{i,j,k} + v_{i+1,j,k})$$

$$w = \frac{1}{2}(w_{i,j,k} + w_{i+1,j,k})$$

It is assumed that:

$$\text{grad } u = \frac{1}{2}(\text{grad } u|_{i,j,k} + \text{grad } u|_{i+1,j,k}) \tag{11}$$

grad v , grad w is defined similarly.

In this way , we only need to calculate grad u , grad v , grad w one time for each cell, and can utilize geometric parameters already defined.

According the definition of gradient:

$$\text{gradf} = \lim_{Vol \to 0} \frac{\int_\Gamma f \, d\vec{s}}{Vol}$$

we have:

$$\text{grad } f \approx \frac{1}{Vol}\sum_{l=1}^{6} f_l \vec{s}_l \tag{12}$$

Where $\vec{s}_i$ is the cell face area vector, f_l stands for function value at face *l*.

Application to u,v,w lead to :

$$\begin{aligned}\text{grad } u &= \frac{1}{Vol}\sum_{l=1}^{6}[\vec{i}u_l s_{lx} + \vec{j}u_l s_{ly} + \vec{k}u_l s_{lz}] \\ &= g_{u1}\vec{i} + g_{u2}\vec{j} + g_{u3}\vec{k}\end{aligned} \tag{13a}$$

and

$$\text{grad } v = g_{v1}\vec{i} + g_{v2}\vec{j} + g_{v3}\vec{k} \tag{13b}$$

$$\text{grad } w = g_{w1}\vec{i} + g_{w2}\vec{j} + g_{w3}\vec{k} \tag{13c}$$

Finally the shear stress is expressed as:

$$\begin{aligned}\vec{F} &= \mu\frac{\partial \vec{q}}{\partial n} + \mu \text{ grad } q_n \\ &= \mu[\vec{i}(n_x g_{u1} + n_y g_{u2} + n_z g_{u3} + n_x g_{u1} + n_y g_{v1} \\ &\quad + n_z g_{w1}) \\ &\quad + \vec{j}(n_x g_{v1} + n_y g_{v2} + n_z g_{v3} + n_x g_{u2} + n_y g_{v2} \\ &\quad + n_z g_{w2}) \\ &\quad + \vec{k}(n_x g_{w1} + n_y g_{w2} + n_z g_{w3} + n_x g_{u3} + n_y g_{v3} \\ &\quad + n_z g_{w3})] \\ &= \mu\{\vec{i}[n_x(2g_{u1}) + n_y(g_{u2} + g_{v1}) + n_z(g_{u3} + g_{w1})] \\ &\quad + \vec{j}[n_x(g_{v1} + g_{u2}) + n_y(2g_{v2}) + n_z(g_{v3} + g_{w2})] \\ &\quad + \vec{k}[n_x(g_{w1} + g_{u3}) + n_y(g_{w2} + g_{v3}) + n_z(2g_{w3})]\} \\ &= \mu\{\vec{i}(n_x g_{11} + n_y g_{12} + n_z g_{13}) \\ &\quad + \vec{j}(n_x g_{21} + n_y g_{22} + n_z g_{23}) \\ &\quad + \vec{k}(n_x g_{31} + n_y g_{32} + n_z g_{33})\} \\ &= Fx\vec{i} + Fy\vec{j} + Fz\vec{k}\end{aligned} \tag{14}$$

In above: $g_{11} = 2g_{u1}$,

$g_{12} = g_{21} = g_{u2} + g_{v1}$,

$g_{13} = g_{31} = g_{u3} + g_{w1}$

$g_{22} = 2g_{v2}$,

$g_{23} = g_{32} = g_{v3} + g_{w2}$,

$g_{33} = 2g_{w3}$

Practically only following six parameters are needed to be computed and stored for each cell:

$$\left.\begin{aligned} g_{11} &= \frac{2}{Vol}\sum_{l=1}^{6} u_l S_{lx} \\ g_{12} &= \frac{1}{Vol}\sum_{l=1}^{6}(u_l S_{ly} + v_l S_{lx}) \\ g_{13} &= \frac{1}{Vol}\sum_{l=1}^{6}(u_l S_{lz} + w_l S_{lx}) \\ g_{22} &= \frac{2}{Vol}\sum_{l=1}^{6}(v_l S_{ly}) \\ g_{23} &= \frac{1}{Vol}\sum_{l=1}^{6}(v_l S_{lz} + w_l S_{ly}) \\ g_{33} &= \frac{2}{Vol}\sum_{l=1}^{6}(w_l S_{lz}) \end{aligned}\right\} \tag{15}$$

Their values at cell face are determined by simple averaging the values of adjacent cells.

Now looking back to the definition of

$$\hat{p} = p + \frac{2}{3}\mu \text{div} \cdot (\vec{q})$$

,the divergence

$$\text{div } \vec{q} = \lim_{Vol \to 0} \frac{\oint_\Gamma \vec{n} \cdot \vec{q} \, ds}{Vol}$$

can be discretized as:

$$\begin{aligned}\text{div}(\vec{q}) &= \frac{\sum_{l=1}^{6}(\vec{q} \cdot \vec{s})_l}{Vol} \\ &= \frac{1}{Vol}\sum_{l=1}^{6}(u_l S_{lx} + v_l S_{ly} + w_l S_{lz}) \\ &= \frac{1}{2Vol}(g_{11} + g_{22} + g_{33})\end{aligned}$$

The $\hat{p}$ can be obtained as:

$$\hat{p} = p + \frac{\mu}{3Vol}(g_{11} + g_{22} + g_{33}) \qquad (16)$$

To sum up , the calculation of shear stress is only requiring computation of six parameters mentioned above . It is really a great reduction on CUP time.

Grid Generation Method

For integrity, the method of forming circular–to–rectangular transition surface is briefly discribed here. The coordinate system is shown in Fig.1.

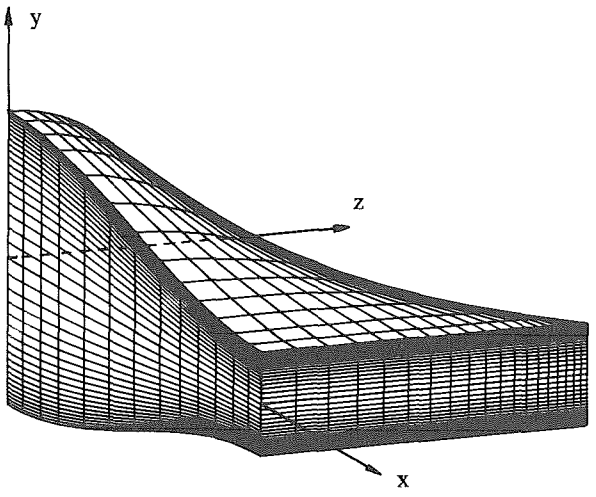

Fig.1 Coordinate System and Surface Grid

Since a circle, an ellipse and a rectangle are all special cases of superellipse. the transition duct can be formed by connecting a series of superellipse cross sections to achieve the geometric smoothness. A general superellipse is defined by the equation

$$\left(\frac{y}{a}\right)^{\eta} + \left(\frac{z}{b}\right)^{\eta} = 1 \qquad (17)$$

When $\eta = 2$,equ.(17) defines a circle while a=b, or otherwise an ellipse. When η is going to be infinite, equ.(17) defines a rectangle with height ofa and width of b.

The area enclosed by a superellipse can be obtained from the equation

$$A_{cs} = \frac{\Gamma\left(\frac{1}{\eta}\right)^2}{\Gamma\left(\frac{2}{\eta}\right)}\left(\frac{\eta}{2}\right)(4ab) \qquad (18)$$

where Γ refers to the "gamma function" and is defined as

$$\Gamma(\eta) = \int_0^{\infty} (d^{-t} t^{\eta-1})dt \quad (\eta > 0) \qquad (19)$$

which can be accurately calculated using standard procedures of orthogonal expansion, say, Chebyshev polynomial expansion, for instance.

The cross section area A_{cs} , the minor and major axes a,b are functions of x in general and must be determined first for the design of transitions. For present used configurations, all the areas of three transition ducts are held constant while the axes a and b are constrained according to the equations

$$a(x) = R-(R-H)(x/L)^2[3-2(x/L)]$$
$$b(x) = R-(R-W)(x/L)^2[3-2(x/L)]$$

Where L is the duct length, R denotes the radius of entrance, W and H are the rectangle width and height of transition exit respectively.

Once A_{cs} , a(x) and b(x) are known, the transition surface is determined by finding out $\eta(x)$ from equ.(18). For practical computation, a rectangle ($\eta = \infty$) can be accurately approximated with $\eta = 100$.

After determining the transition shape, we proceed to grid generation. Usually, an "O" type grid is preferred for circle kind ducts, however it concentrates too many points on the centre and is deficient for rectangular section. "H" type grids have the advantage of grid efficiency and is especially suitable for rectangular section, but it is not easy for conventional method to generate a satisfactory grid fitting well to the circular section.

Since grid quality has great impact on computation results, a new grid generation method has been contrived for this particular kind of duct. This method basically breaks the 3d grid into a number of 2d grids which are generated on each cross section and related to each other through analytic transformation, therefore the smoothness of this composite grid is guaranteed. The main idea is presented as follows.

The equ.(17) , defines the general cross section shape of the duct and nozzle, can be rewritten in complexion function form as

$$\zeta = \left[\left(\frac{\cos\alpha}{a}\right)^{\eta} + \left(\frac{\sin\alpha}{b}\right)^{\eta}\right]^{-\frac{1}{\eta}} e^{i\alpha} \qquad (20)$$

where α is the imaginary angle, $i = \sqrt{-1}$.

The grids on this section are obtained through following procedure.

First, prechoose the basic grids on a square (a=1,b=1). The grids are formed by simply dividing the square using two families of orthogonal straight lines. The grid number and thickness distribution at each direction can be determined just according to your requirement .

The second step is to map the square onto a unit circle. The process is discribed briefly as follows.

For $\zeta_{circle} = [(\cos\alpha)^2 + (\sin\alpha)^2]^{-\frac{1}{2}} e^{i\alpha}$

and $\zeta_{square} = \left|[\cos\alpha)^{\eta} + (\sin\alpha)^{\eta}]^{-\frac{1}{\eta}}\right|_{\eta\to\infty} e^{i\alpha}$

Their relation is found by setting that the imaginary angles keep unchange during the mapping as corresponding grid points

$$\zeta_{circle} = \left|\cos^{\eta}\alpha + \sin^{\eta}\alpha\right]^{\frac{1}{\eta}}\Big|_{\eta\to\infty} \zeta_{square} \qquad (21)$$

Therefore the grid point on the unit circle can be found using the formula above from the corresponding point ζ_{square} on the square.

The third step is to map the unit circle onto a superellipse with exponential of η using the relation

$$\zeta_{supere}[\mathrm{Cos}^{\eta}\alpha + \mathrm{Sin}^{\eta}\alpha]^{-\frac{1}{\eta}} = \zeta_{circle} \qquad (22)$$

For each grid point $\zeta_{circle}(y+iz)$ on the circle, we can find out the correspondent point $\zeta_{supere}(y+iz)$ from equ.(22).

The forth step is to sketch the unit superellipse $\zeta_{supere}$to the general superellipse with minor and major axes of a and b. This will be done by a simple extension transformation

$$y_{new} = a y_{supere} \qquad (23a)$$

$$z_{new} = b z_{supere} \qquad (23b)$$

For any cross section with given η,a,b , repeating 3rd and 4th step, then the grid is generated. It can be easily confirmed that the boundary point(y_{new},z_{new}) transformed from equ.(23) is content to equ.(17).

The grids generated using present method in different sections of transition duct are shown in Fig.2–4, the surface grid is given in Fig. 1. It can be seen that the grid on rectangle is of surely orthogonal "H" type, when on circle section, it possesses the "O" type grid character but dose not concentrate on the centre. The whole grid is smooth and almost orthogonal. The thickness distribution of grid is easily controlled through adjusting the basic grid. The success of this kind of grid is further confirmed by the satisfactory computational results discribed later.

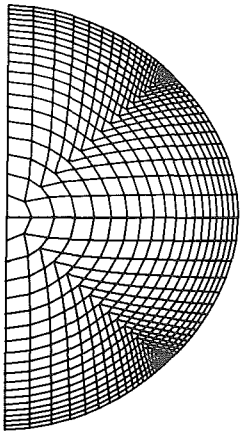

Fig.2 Grid on the Entrance Cross Section

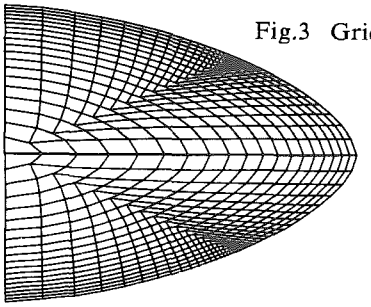

Fig.3 Grid on Mid–Section

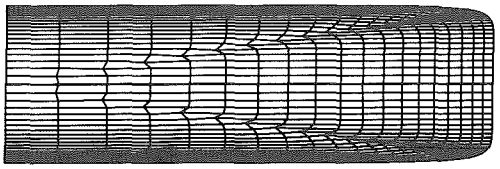

Fig.4 Grid on Rear Section of Transition Duct

Turbulence Model

For simplicity, the algebraic eddy viscosity model of Baldwin and Lomax is applied. The attraction of the model is that it does not require the determination of the edge of the boundary layer in N–S computation. Before we introduce the modification in 3d computation, the original model cited here.

For the inner region of the shear layer, the eddy viscosity is given by

$$\mu_{t,i} = \rho l^2 |\omega| \qquad (24)$$

where

$$l = 0.4y[1 - \exp(-y^{+}/26)] \qquad (25)$$

$$y^{+} = \sqrt{\rho_w \tau_w}\, y/\mu_w \qquad (26)$$

and ω is the vorticity.

In the outer region, the eddy viscosity is given by

$$\mu_{t,o} = \rho K C_{cp} F_w F_{kleb} \qquad (27)$$

where K is the Clauser constant, C_{cp} is the constant given in [5], and

$$F_w = \mathrm{minimum}(y_{max}F_{max}, C_{wk}y_{max}U_{diff}^2/F_{max}) \qquad (28)$$

where C_{wk} is a constant. The quantities $y_{max}$and $F_{max}$are determined from

$$F(y) = y|\omega|[1 - \exp(-y^{+}/26)]$$

$F_{max}$is the maximum value of F(y) that occurs in a profile and $y_{max}$is the value of y at which F_{max}occurs. The function F_{kleb}, the Klebanoff intermittency factor, is determined from

$$F_{kleb} = \left[1 + 5.5\left(\frac{C_{kleb}}{y_{max}}\right)^6\right]^{-1} \qquad (29)$$

where y is the normal distance to the surface and $C_{kleb}$is a constant. $U_{diff}$is the difference between the maximum and minimum velocity magnitudes in a profile.

The original model is basically proposed for one wall case, but the internal flow inside a duct is a flow between walls, The eddy viscosity is theoretically effected by each of the walls. therefore adaptation to the original model must be made.

Because of the full symmetry of the considered configurations, only one forth of the flow domain is actually computed. Practically we are calculating the turbulent flow in a corner of two walls with the other two side of symmetric planes. In this case, the normal

distance y used in equ.(25) and (26) are suggested to be replaced by

$$y=\frac{2Y_1Y_2}{Y_1+Y_2+\left(Y_1^2+Y_2^2+2Y_1Y_2\,Cos\gamma\right)^{\frac{1}{2}}} \tag{30}$$

where Y_1, Y_2 are the distances to the two wall respectively, γ is the angle included between the two walls. The formula suggested above is established according the following facts.

First, if the two walls cross at a right angle, equ.(30) becomes Buleev's mixing length

$$y=\frac{2Y_1Y_2}{Y_1+Y_2+\left(Y_1^2+Y_2^2\right)^{\frac{1}{2}}} \tag{31}$$

as used in[9].

Second, when the cross section is a circle, the angle γ between walls is approximately equal to π. Then the formula reduced to

$$y=\frac{2Y_1Y_2}{Y_1+Y_2+|Y_1-Y_2|}=\text{minimum}(Y_1,Y_2) \tag{32}$$

,It conforms with the definition of original model in cylindrical coordinate system.

Third, when γ increased, y increases. This is to say that the integrated effects of two wall on eddy viscosity decrease . It is in conformity to physical fact.

After redefining the y, there are still problems existed in selection of which wall is used in the calculation of μ_t where the μ_w,ρ_w and τ_w in equ.(26) are defined. In some of references, this problem is avoided by calculating two sets of eddy viscosity respecting to the two walls then taking the minor one. This kind of treatment is obviously unreasonable for it ignores the different degree that thetwo walls affect the $\mu_t$on a specific point. Really the effective degree of each wall could be measured approximately by a virtual length as

$$\left.\begin{aligned}\bar{y}_m&=Y_m[1-\exp(-\bar{y}^+/26)]\\ \bar{y}^+&=\frac{\sqrt{\rho_w\tau_w}}{\mu_w}Y_m\end{aligned}\right\}\quad(m=1,2) \tag{33}$$

where y_m is the distance to the wall m. The bigger the $\bar{y}$,the less the wall has influence on the point. Therefore, the selection principle could be formed as:

For a given point , its μ_t is determined from the wall which holds the minor $\bar{y}$.

Substantially, the equ.(30) is constructed to consider the combined influence of the two walls, and the selection principle is used to determine of which wall the ρ_w, $\tau_w$and $\mu_w$are used in equ.(26).

Boundary Condition

At inflow boundary, the total pressure and total enthalpy are held constant and the flow angles fixed. For subsonic inflow as in present cases, thevelocity is extrapolated from the interior. The static pressure and densityare obtained from gasdynamic relations.

At the outflow boundary, since the main flow is supersonic, no condition is prescribed, all the variables are extrapolated . In the region of boundarylayer, if the flow is subsonic, the static pressure is determined from the assumption of zero normal gradient of pressure. The other flow variables are still extrapolated from interior points.

In the symmetric planes, the mirror reflection treatment is used. An alternate method is to treat the plane as a slip boundary with zero cross fluxes, only pressure is needed to extrapolated from interior .

For wall surface, no–slip condition is imposed. As cell faces lie along the surface, the fluxes of mass, momentum and energy across the faces are set to zero. The surface pressure is simply extrapolated from interior. The shear stress is found from an improved wall functions formula derived by the first author in [4] as

$\tau_w=q/y$ if $y^+\leqslant 11.225$,

or otherwise

$$\tau_w=(2aq\kappa\sqrt{\rho_w\tau_w})^{\frac{a}{1+2a}},\quad a=(2\,logEy^+)^{-1}$$

where $E=9.793$,$\kappa=0.4187$. The formula has been confirmed very efficient in [7,8].

The use of wall functions can reduce the need of severe mesh refinement near wall, and satisfactory results could be achieved even on relative coarse grids.

Result and Conclusion

Three transition ducts with length of 0.5,0.75 and 1 times of entrance diameter(denoted by d), integrated with a convergent–divergent nozzle through a short uniform duct connection, are investigated in present study. The ratio of width to height of transition exit is as high as 6.33. The same models have been tested in the static test facility of Langley 16–Foot Transonic Tunnel, NASA [3]. Their geometric details refer to [3]. By virtue of the full symmetry of the configurations and axial inflow conditions, only one forth of the internal region is actually needed to calculate. The grid number for the one–quarter–domain is $56\times 16\times 18$ with clustering to the wall. A typical iteration number of 800 is needed to reduce the maximum residual three orders of magnitude for turbulent flow computation, and only half the iterations for a converged Euler solution. All this calculation is completed on a personal computer.

Fig.5–7 show the computed static pressure ratio distribution and comparison with the experimental data. For the case of $L/d=1$, because there is no separation observed both experimentally and numerically (refer to Fig.8,11) in the transition duct, the Euler solv-

er gives good enough results. However N–S solution dose show improvement in the region of sidewall where viscosity becomes dominating. When the L / d reduced to 0.75, as shown in Fig. 6, the Euler solution still remains valid for most region except in the rear parts of both transition duct and nozzle sidewalls. In this case, a small region of separation occurred in the vicinity of sidewall centerline and near the exit of transition duct (refer to Fig. 9,12). Significantly, the N–S solver almost reproduces the experimental results. Once again, the N–S solution accurately matches the test data in the case of L / d = 0.5 as shown in Fig. 7, but the Euler solution has a big deviation from the measurement along sidewall, implying the separation is becoming severe.

It is needed to mention that the computed pressure is in a higher overall level than the measured. It is believed that the overall error may be due to the difference of reference total pressure p_t between the experiment and computation. The total pressure pt is defined at the exact entrance of transition duct in the present study, but in the test, it is measured in average at a station much more upstream.

Fig. 8,9,10 show the 3d view of the near–surface velocity vectors. It is easy to find that there is no separation for the case of L / d = 1. When the relative length of transition duct reduced to 0.75, the separation begins at the rear part of transition duct sidewall. The result is congruous with the test. If the length is further decreased to 0.5, the flow separates immediately when the sidewall begins expanding as shown inFig.10. Two pairs of vortexes are formed after separation along the sidewall. The separation causes velocity profile deficit near sidewall throughout the nozzle. resulting significant loss of internal performance.

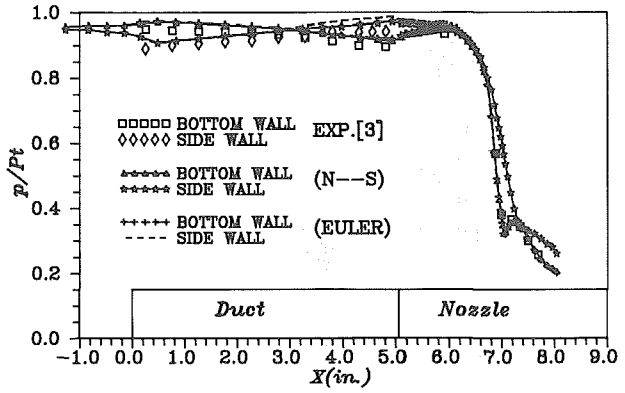

Fig.5 Comparison of Experimental and Calculated Results for Configuration with L / d = 1

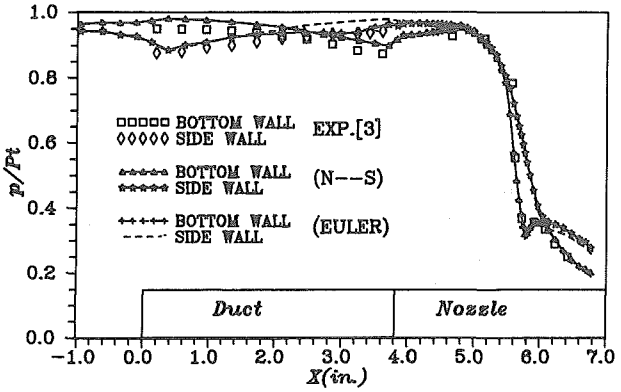

Fig.6 Comparison of Experimental and Calculated Results for Configuration with L / d = 0.75

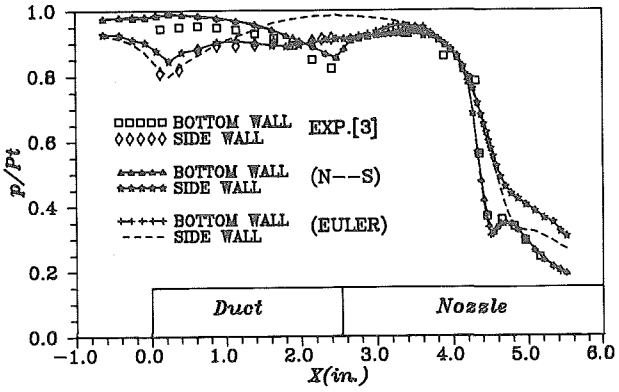

Fig.7 Comparison of Experimental and Calculated Results for Configuration with L / d = 0.5

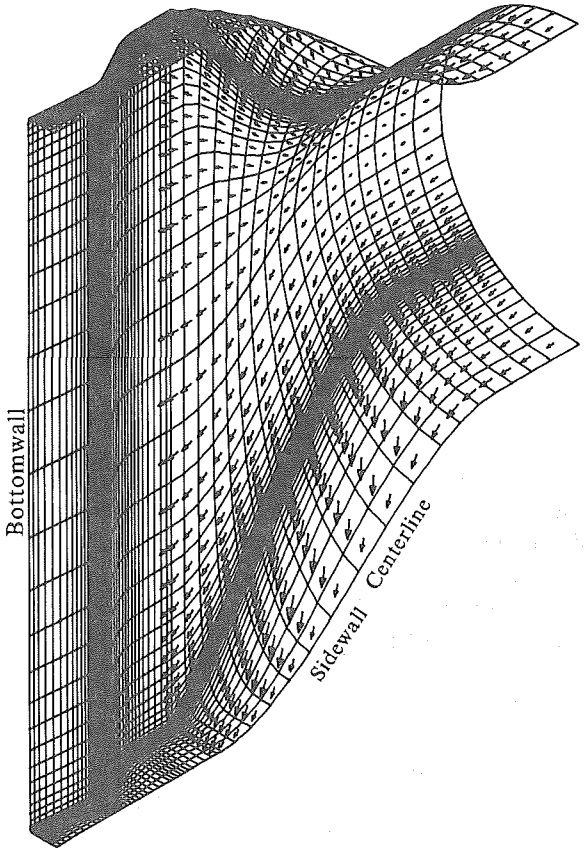

Fig.8 3D View of Near–Surface Velocity Vectors on Half of Configuration with L / d = 1

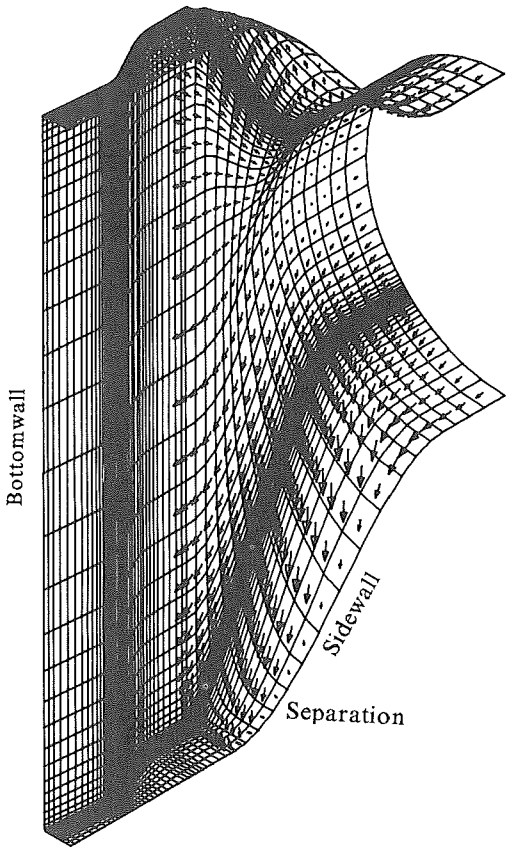

Fig.9 3D View of Near–Surface Velocity Vectors on Half of Configuration with L / d = 0.75

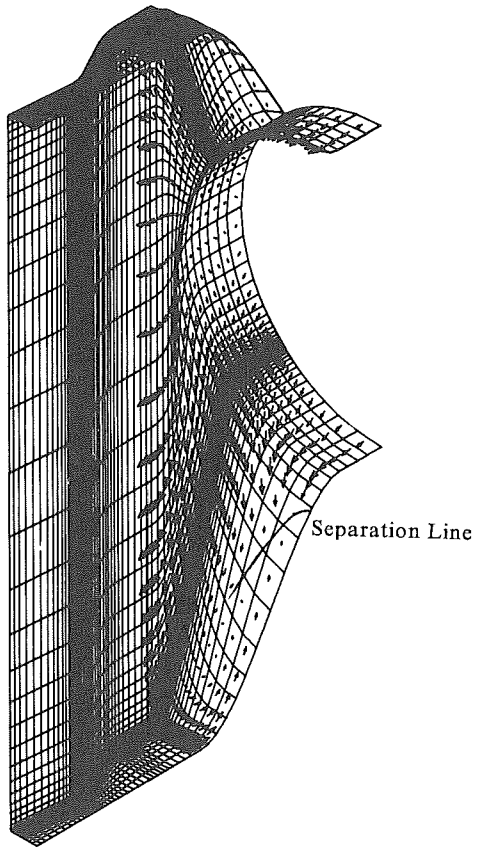

Fig.10 3D View of Near–Surface Velocity Vectors on Half of Configuration with L / d = 0.5

To have a clear view of the internal flow patterns, the velocity vectors are also plotted on the symmetric plane of sidewall–to–sidewall. Fig.11 shows the tangential component vectors on this divergent plane for the case of L / d = 1. The flow is in a normal style. Fig 12 shows the case of L / d = 0.75, small region of separation is easy–seeing. The near–sidewall flow after separation is in a centripetal direction, indicating that strong secondary flow exists. When the relative length L / d is reduced to 0.5, as shown in Fig.13, the situation becomes more severe, since the separated flow, occupied a considerable area, causes much stronger secondary flow in a pattern of one pair of vortex in each sidewall nearby.

On the another symmetric plane (bottom–to–bottom), the velocity vector fields of three configurations have no essential difference. For the conciseness, only one such plot is given in Fig.14 for L / d = 0.5.

Mach number contours on the two symmetric planes are illustrated in Fig.15–20 for all configurations. Since such contours for similar configurations are not found from available references, no comparison is made here. All the contours have the same feature that the iso–Mach lines concentrate in the nozzle throat region , owing to the rapid acceleration of speed. For same reason, the boundary layer is thin and the effect of viscosity is in a low altitude in the area. Except in the separation region, the respective contours for different configurations are in a similar fashion.

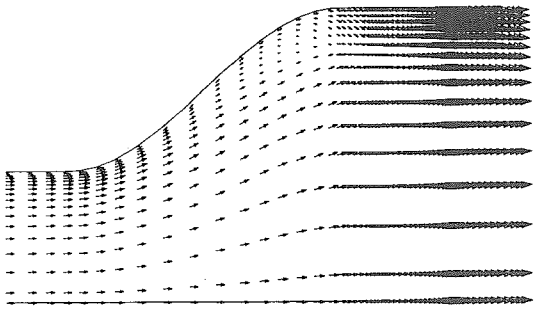

Fig.11 Vector on Symmetric Plane (S–S) with L / d = 1

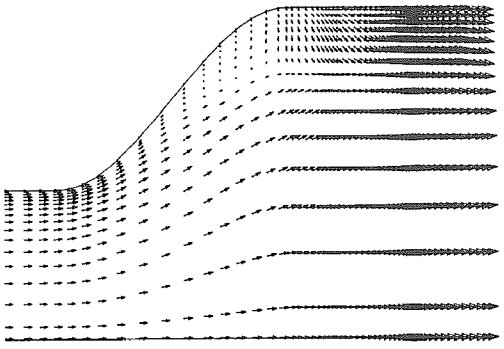

Fig.12 Vector on Symmetric Plane (S–S)
with L / d = 0.75

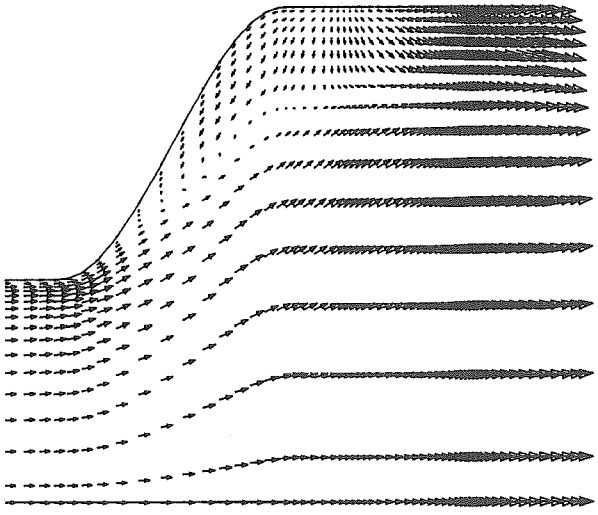

Fig.13 Vector on Symmetric Plane (S–S)
with L / d = 0.5

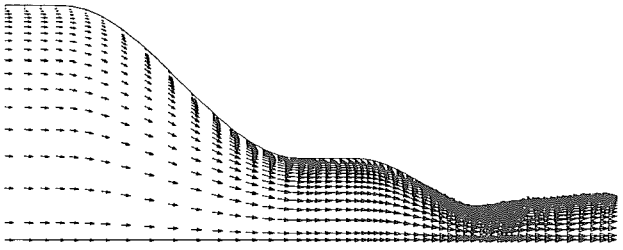

Fig.14 –Vector on Symmetric Plane (B–B)
with L / d = 0.5

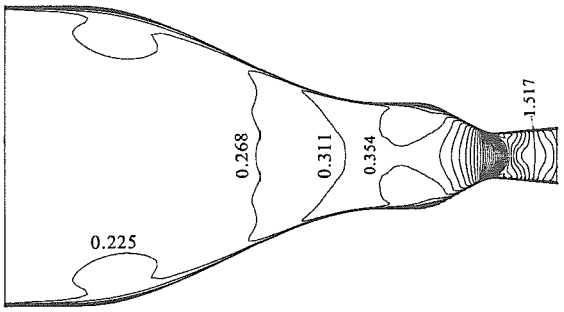

Fig.15 Mach Number Contour ($\delta m = 0.043$)
on (B–B) Plane with L / d = 1

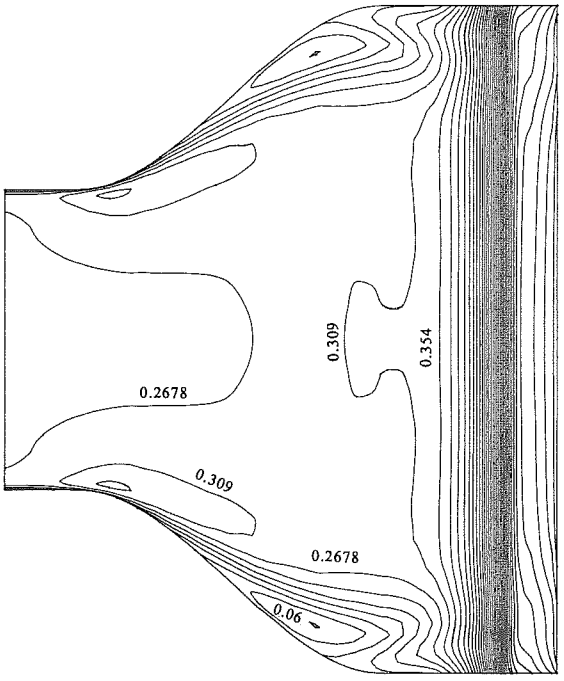

Fig.16 Mach Number Contour ($\delta m = 0.0414$)
on (S–S) Plane with L / d = 1

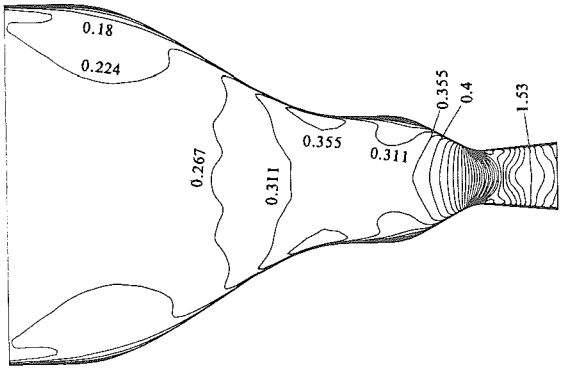

Fig.17 Mach Number Contour ($\delta m = 0.0435$)
on (B–B) Plane with L / d = 0.75

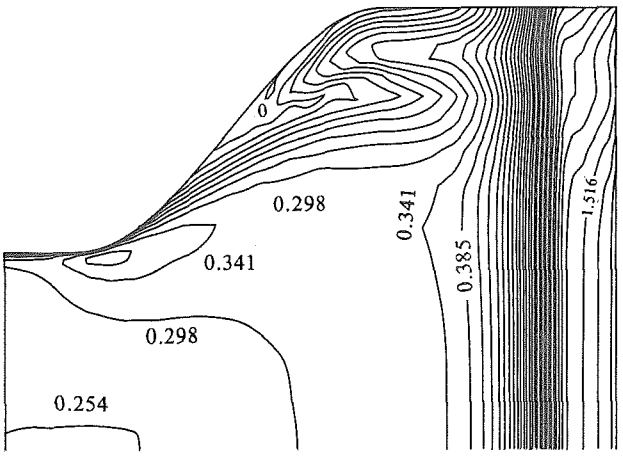

Fig.18 Mach Number Contour ($\delta m = 0.0425$) on (S–S) Plane with L / d = 0.75

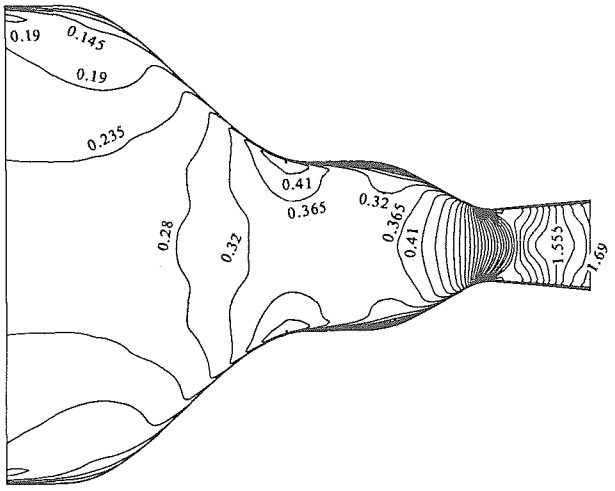

Fig.19 Mach Number Contour ($\delta m \approx 0.045$) on (B–B) Plane with L / d = 0.5

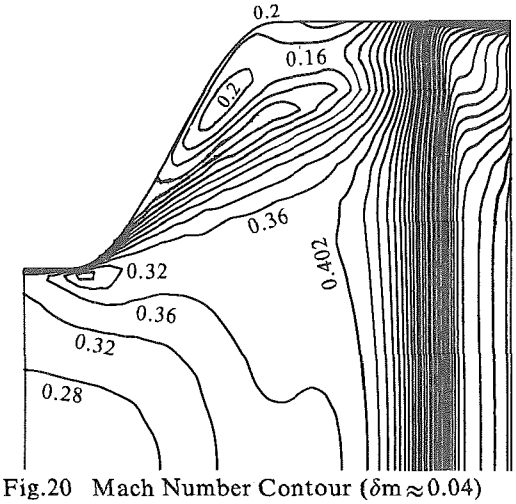

Fig.20 Mach Number Contour ($\delta m \approx 0.04$) on (S–S) Plane with L / d = 0.5

Reference

1. Capone,F.J., "Static Performance of Five Twin–Engine Nonaxisymmetric Nozzles with Vectoring and Reversing Capability", NASA TP–1224,1978.
2. Steven, H.L., Thayer, E.B. and Fullerton, J.F., "Development of the Multi–Function 2–D / C–D Nozzle", AIAA–81–1491, July 1981.
3. Burley Ⅱ, J.R., Bangert, L.S. and Carlson J.R., "Static Investigation of Circular–to–Rectangular Transition Ducts for High–Aspect–Ration Nonaxisymmetric Nozzles", NASA TP–2534, 1986.
4. Zheng,Qiaoqing, "Integrated Flowfield Analysis Methodology for Fighter Forebody–Inlet Combinations", Ph.D Thesis, Northwestern Polytechnical University, 1990.
5. Baldwin, B. and Lomax, H., "Thin Layer Approximation and Algebraic Model for Separated Turbulent Flows", AIAA 78–257, 1978.
6. Jameson, A., Schmidt, W. and Turkel, E., "Numerical Solution of Euler Equations by Finite Volume Methods Using Runge–Kutta Time–Stepping Schemes", AIAA 81–1259,1981.
7. Zheng, X., Xu, Y. and Chen, N., "Aerodynamic Calculation of Turbomachine Cascade Flows with Shocks Using Euler and Navier–Stokes Solvers", **Computational Mechanics**,Y.K. Cheung, et.al. ed., Balkema / Rotterdam / Brookfield Publications, Vol.2, pp.1505–1510,1991.
8. Chen, N., Zheng, X. and Xu. Y., "Numerical Computations of Turbomachinary Cascade Turbulent Flows With Shocks by using Multigrid Scheme", ICAS–92–3.1.3, The 18th ICAS Congress, Sept. 1992, Beijing, China.